Theory for Radii and Second Virial Coefficients. 1. Highly Charged Polyelectrolytes

Dirk Stigter and Ken A. Dill*

Department of Pharmaceutical Chemistry, University of California, San Francisco, California 94143

Received July 22, 1994; Revised Manuscript Received March 10, 1995[⊗]

ABSTRACT: We develop a theory for the dependence of the radii of gyration and second virial coefficients of highly charged polyelectrolytes on molecular weight and ionic strength. The theory is based on using (i) the Flory–Fisk[1] distribution of chain conformations to describe the elastic entropy and (ii) a charged rod model of local intrachain repulsions based on the full Poisson–Boltzmann equation. To describe the overlap between two approaching chains, we go beyond the rigid sphere model of Orofino and Flory[2] and assume the chains can change coil size and can deform as elastic ellipsoids to avoid unfavorable interchain repulsions. Added salt weakens electrostatic repulsions, leading to reduced radius of gyration and second virial coefficients. Without adjustable parameters this approach gives reasonable agreement with data on T7 DNA, Col E1 DNA, and poly(styrenesulfonate)s over two decades of ionic strength.

1. Introduction

We develop a model for the conformations of individual polyelectrolyte molecules and for interactions between pairs of polyelectrolyte chains. There is a substantial body of theoretical work on chain expansion and virial coefficients of polymers; it is reviewed by Yamakawa,[3] Fujita,[4] and des Cloizeaux and Jannink.[5] There has been much less modeling of polyelectrolytes. Here we give a brief history of theories of polyelectrolyte conformations. Models fall into different categories. First, some treatments consider chains in salt-free solutions[6–9] and model the electrostatics using Coulomb's law, whereas others treat the shielding of charge due to added salt. Since most realizable polymer experiments and most biopolymer solutions involve added salt, our interest here focuses on the case of added salt. Second, some models treat added salt at the full Poisson–Boltzmann (PB) level, others at the level of the linear (Debye–Hückel) approximation to it (sometimes called the screened Coulomb interaction). Third, polyelectrolyte chains have been treated as having zero thickness or as flexible rods with finite thickness.

An early theory of coil expansion of polyelectrolytes was by Hermans and Overbeek,[10] who assumed an isolated polyelectrolyte molecule is a charged porous sphere. They treated the electrostatics by solving the linearized Poisson–Boltzmann equation based on assuming spherical symmetry of the whole polyelectrolyte chain. An alternative approach recognizes that polyelectrolytes have another important length scale: the persistence length of the chain. Already in 1951 Alfrey et al.[11] and Fuoss et al.[12] recognized that local regions of highly charged polyelectrolyte chains act as relatively stiff rods, due to the strong charge repulsions. In the 1970s Odijk,[13] Odijk and Houwaart,[14] and Skolnick and Fixman[15] invoked Debye–Hückel electrostatics. This work involves a major shift of paradigm, from treating the spherical symmetry of the whole molecule to treating the *cylindrical symmetry* of each chain *segment*, assumed to be locally rodlike. Odijk[13,14] and Skolnick and Fixman[15] further assumed (i) that the chain is an infinitely thin line of charge and (ii) that the persistence length of the chain is the sum of intrinsic and electrostatic components. Assumption ii is well-suited for stiff highly charged chains such as DNA, although it may be poorer for more flexible chains.[7] The treatments of Odijk[13,14] and Skolnick and Fixman,[15] based on the linearized Poisson–Boltzmann equation, predicted that for weakly charged polyelectrolytes the electrostatic persistence length, P_{el}, scales with ionic strength, I, as $P_{el} \sim I^{-1}$. For highly charged polyelectrolytes, such as DNA, an important step forward was the more recent work of Fixman[16] and Le Bret,[17] who computed the electrostatic persistence length at the level of the full Poisson–Boltzmann equation; i.e., they treated highly charged cylinders of finite radius with a perturbation expansion in the curvature of the rod. These treatments show that for the electrostatic persistence length of highly charged polyelectrolytes there is no simple scaling law with ionic strength[17] as in the simpler model described above, and the experimental data are in better agreement with the treatments of Fixman[16] and Le Bret.[17] Thus for modeling the flexibility of highly charged polyelectrolytes, a finite chain radius is important and the Debye–Hückel approximation is not adequate; the full PB equation is required.

To compute polyelectrolyte coil radii, Stigter[18,19] adopted the treatments of Le Bret[17] and Fixman[16] for the electrostatic persistence length and used the chain statistics of Hermans and Overbeek[10] to account for chain retractive forces. In the present work, we now replace the Hermans–Overbeek statistics with a different model that has been used to treat chain collapse processes in homopolymers[20] and heteropolymers and proteins,[21,22] based on the Flory–Fisk distribution function[1] and the Flory excluded volume approximation.[23] An advantage of studying highly charged polyelectrolytes, rather than neutral polymers, is that since electrostatics dominates, adjustable parameters describing short-ranged interactions, such as the Flory–Huggins χ parameter, are not required. We study the effects of coil size fluctuations by comparing the rms radius of gyration with the most probable (minimum free energy) coil size. For uncharged polymers these effects have been reviewed by Yamakawa[3] and discussed more recently by Birshtein and Pryamitsyn.[24]

There has not been much study of the pair interactions between polyelectrolyte chains in dilute solution. Theory for second virial coefficients of polyelectrolytes

[⊗] Abstract published in *Advance ACS Abstracts,* July 1, 1995.

0024-9297/95/2228-5325$09.00/0

Table 1. Scaling Factor s in Charge se per DNA Phosphate and Effective Diameter d_B (Å)

M_{NaCl}	s_{rod}	$s_{line\ charge}$	d_B[a]	d_B[b]
0.5	0.630	4.36	34.1	35.4
0.2	0.568		44.0	46.6
0.1	0.515	1.024	56.2	62.9
0.05	0.463		74	87
0.04		0.644	81.6	
0.02	0.399	0.499	112	138
0.01	0.359	0.409	157	200
0.005	0.325	0.350	223	293
0.002	0.289	0.300	363	490

[a] Poisson-Boltzmann model from Stigter[27] and Stigter and Dill.[34] [b] Debye–Hückel model from Fixman and Skolnick.[26]

was first developed by Orofino and Flory,[2] assuming that overlapping coils retain their (average) spherical symmetry. For uncharged polymers Gobush et al.[25] found that allowing ellipsoidal coil shapes reduces the predicted second virial coefficients significantly. This reduction is confirmed by our calculations for polyelectrolytes. To complete the frame for the present work, we review in more detail the electrostatics used in our kinked rod model, some Monte Carlo simulations, and relevant aspects of chain statistics.

2. Electrostatics of the Rod Model

We first discuss the excluded volume of two rod segments that are separated in the chain sequence. Our treatment of excluded volume rests on the pair repulsion (second virial coefficient) between charged rods. This repulsion may be approximated by modeling the chain as an uncharged flexible rod with an effective diameter, d_B, which depends on the polyelectrolyte charge and on the Debye length in the surrounding salt solution. The distance between adjacent phosphate charges on duplex DNA is much smaller than the Debye length in salt solutions of interest. Therefore, the far electrostatic field around DNA, required for the interaction between rod segments, can be well reproduced by representation as a rod with a smeared surface charge. This is the basis for the Fixman–Skolnick theory,[26] which models segments as charged rods with a Debye–Hückel ionic atmosphere. However, DNA will have a sufficiently high charge density that the Debye–Hückel approximation does not adequately predict ion distributions close to the rod, and this is important in the present work for obtaining the correct effective diameter of the chain. The evidence for this is as follows.

Stigter[27] has applied the full Poisson–Boltzmann equation to obtain effective diameters by using the Debye–Hückel potential with a scaled polyelectrolyte charge. He evaluated the effective diameter d_B of a B-DNA rod with radius $a = 12$ Å and a smeared surface charge corresponding to -0.73 e per DNA phosphate, as found from electrophoretic experiments in NaCl solutions by Schellman and Stigter.[28] Column 2 of Table 1 gives the scaled DNA charge per phosphate group used in these calculations, and column 4 the Poisson–Boltzmann values of d_B. The scaling factor, s, varies not only with the salt concentration but also with the radius a of the rod. For example, for $a = 0$, a line charge, column 3 of Table 1 gives the corresponding scaled charge per DNA phosphate. With the screened Debye–Hückel interaction potential, both models, Debye–Hückel and full Poisson–Boltzmann, give the same far potential field and, hence, the same d_B. The difference between the two sets of s values is due to the countercharge in the cylindrical volume with radius 12 Å around the line charge. Table 1 also compares the effective chain diameters predicted by the full Poisson–Boltzmann treatment[27] and the Fixman–Skolnick Debye–Hückel treatment.[26] At high salt differences are small, but at low salt the Fixman–Skolnick results for d_B are significantly higher than experimental values.[29,30] Also consistent with the full Poisson–Boltzmann treatment is the following evidence. The effective diameters d_B of B-DNA in Table 1 based on the Poisson–Boltzmann model are in good agreement with results of three different types of experiments which are not, or only slightly, dependent on the persistence length of DNA: (i) equilibrium sedimentation of short DNA fragments by Brian et al.,[31] (ii) light scattering experiments on short DNA by Nicolai and Mandel[32] (see also Fixman[33] and Stigter and Dill[34]), and (iii) experiments on the probability of knots in P4 DNA by Rybenkov et al.[29,30] and in two other DNA samples by Shaw and Wang.[35] Hence in the present work we use the fully Poisson–Boltzmann treatment.

Table 2. Electrostatic Persistence Length of DNA, P_{el} (Å)

M_{NaCl}	Fixman[a]	eq 1[b]	eq 1[c]
0.5	70	12	221
0.1	96	58	61
0.05	111		
0.04		145	60
0.02	136	291	72
0.01	168	581	97
0.005	214	1162	143
0.002	331	2905	261

[a] From Stigter,[19] as interpolated from tables by Fixman.[16] [b] With $z = 2/3.37$. [c] With $z = (2/3.37)s_{line\ charge}$.

How should we treat the persistence length of polyelectrolytes? The usual assumption is that the total persistence length, P, is the sum of an intrinsic part, P_{intr}, and an electrostatic contribution, P_{el}. In 1977 Odijk[13] and, independently, Skolnick and Fixman[15] derived an analytical expression for P_{el} based on the model of a flexible line charge with Debye–Hückel interactions. Their result for P_{el} can be expressed in terms of the charge ze per unit length of the line charge, the Bjerrum length $l_B = e^2/(4\pi\epsilon_0 DkT)$, and the Debye length $1/\kappa$, as:

$$P_{el} = \frac{z^2 l_B}{4\kappa^2} \tag{1}$$

That work was followed in the early 1980s with computations of P_{el} by Le Bret[17] and by Fixman,[16] now based on the DNA model of a flexible rod with a smeared surface charge and a Poisson–Boltzmann double layer. Although the computational approach in the two treatments was somewhat different, both sets of numerical results are consistent with each other. In Table 2 the second column shows P_{el} for B-DNA as a function of ionic strength, as interpolated from Fixman's results for the rod model.[16] The third column of Table 2 gives P_{el} from eq 1 with the full charge density of B-DNA, i.e., two phosphate charges for a rise of 3.37 Å per base pair. As confirmed by Le Bret's comparison with experiments,[17] the rod model is a much more accurate representation of DNA than the line charge. The comparison in Table 2 shows that for highly charged polyelectrolytes at low ionic strength eq 1 seriously overestimates the repulsion between vicinal charges along the chain. We could use charge scaling as a remedy. To demonstrate this, the results in the last column of Table 2 are also based on eq 1, but now using

the scaling factors of Table 1 for the line charge. Although such scaling gives improvement, the results are still unsatisfactory compared with those of the rod model in the second column of Table 2. Therefore, in the present work we have used the theoretical results for rods by Le Bret[17] and by Fixman.[16]

The reasons for the quantitative failure of the line charge model in eq 1 are not entirely clear. The intersegment repulsion in d_B as discussed above depends on the radial component of the electrical field, which is greatly simplified by symmetry. However, in the computation of P_{el} symmetry is of little help. Here we need the effects of chain bending on the intrasegment interactions, and such differential effects are not easily predicted. According to Le Bret,[17] "the persistence length depends on the electrostatic potential at the very surface of the polyion".

Peitzsch et al.[36] have combined the Fixman–Skolnick treatment of segment pair repulsion[26] with the Yamakawa expression for the second virial coefficient (ref 3, eq 21.5). As argued above, for highly charged polyelectrolytes in low salt solutions this approach overestimates the segment pair repulsion. Moreover, the Yamakawa expression is based on a perturbation approach for uncharged polymers which does not distinguish local (persistence length) and nonlocal (excluded volume) interactions in polyelectrolytes. Beyond the data on d_B in Table 1, we have not made a detailed comparison of this approach with our work.

3. Monte Carlo Simulations

With Monte Carlo methods one may study the behavior of several models of polyelectrolytes. The two prevailing types are (i) a sequence of hard cylinders of specified length and diameter and (ii) a sequence of point charges connected by vectors of constant length. The direction of successive cylinder axes or length vectors may be random or subject to certain restrictions of the bending angle. In (i) the diameter of the cylinders simulates their repulsion and the relevant excluded volume, and in (ii) a screened DH potential between scaled charges is often used. In many cases the generation of accurate results for large expansion factors α_s, that is, for long chains, is restricted by computer time. For example, in a type i simulation by Post,[37] the linear expansion factor due to excluded volume was maximal $\alpha_s = 1.072 \pm 0.014$, not quite good enough to discriminate between theories by Manning[38] and Stigter.[18]

In type ii Monte Carlo studies it is difficult to distinguish properly between local and nonlocal electrostatic interactions. There is good evidence (see above) that the nonlocal interactions can be well simulated by a sequence of scaled point charges (see Table 1 for scaling factors appropriate for B-DNA). However, the same scaled charges are quite unsatisfactory for the local repulsions that increase P_{el} (see Table 2, last column). In view of the foregoing it is not surprising that MC simulations of poly(acrylic acid) by Carnie et al.[39] with the full charge e per monomer give results for the persistence length that are far too high. In Table 7 of their paper, Carnie et al.[39] report simulation results for the persistence length $P = 65$ Å at ionic strength $I = 0.1$ M and $P = 290$ Å at $I = 0.01$ M. This compares with our interpolations from the Le Bret[17] tables of $P = 26.7$ Å at $I = 0.1$ M and $P = 65.3$ Å at $I = 0.01$ M. The use of the DH potential with unscaled charges also casts serious doubt on the results for the power law behavior of the radius of gyration as a function of polymer weight by Carnie et al.[39] The foregoing remarks apply also to the simulations of partially ionized polyelectrolytes based on the same defective model by Christos et al.[40]

In general, Monte Carlo results of type ii simulations are suspect because, as pointed out above, the treatment of local interactions (consistent with eq 1 for the persistence length) is defective for high charge densities. For this reason the work of Reed and Reed,[41] and of many authors cited by them, should be reevaluated. An approximate remedy in this type of simulation would be to use for the local repulsions different scaling factors that would be consistent with the Le Bret[17] and Fixman[16] tables. Of course, this would still leave us with the problem of where is the boundary between local and nonlocal interactions.

An interesting approach to this problem of local and nonlocal interactions is in a recent paper by Krishnaswamy and Fixman.[42] They first determine the short chain properties by a Monte Carlo simulation with a type ii model. From the short chain results the long chain expansion is then synthesized with a perturbation method. Finally, these results are compared with Monte Carlo simulations of long chains. The excellent agreement between the two sets of results is, perhaps, not too surprising. As is obvious from our discussion, the main problem in Monte Carlo work on coil expansion is in the short range interactions. In the above work of Krishnaswamy and Fixman[42] any errors in the short range results are propagated into the long chain behavior by their perturbation analysis as well as by the long chain Monte Carlo simulations. In general, type ii models are very suitable for the nonlocal interactions which are quite insensitive to the actual chain configuration: Stigter[18] found little difference between expansion results for three different segment distributions: uniformly spherical, Gaussian spherical, and uniformly ellipsoidal. Finally, we note that in the second virial coefficient we deal only with interaction between chain segments, but not with the more difficult intrasegment interactions.

4. Coil Expansion and Chain Statistics

In this section, we first review the Flory treatment of chain statistics, following Yamakawa.[3] The Gaussian distribution for the radius of gyration is

$$P(r_g)\,dr_g = C \exp\left(-\frac{3}{2}\frac{r_g^2}{\langle r_g^2\rangle_0} - \frac{\Delta F}{kT}\right) r_g^2\,dr_g \qquad (2)$$

where C is the normalization constant. $\langle r_g^2\rangle_0$ is the value of $\langle r_g^2\rangle$ for $\Delta F = 0$, i.e., in a Θ solvent. The coil expansion factor α_s is defined by

$$\alpha_s^2 = \langle r_g^2\rangle/\langle r_g^2\rangle_0 \qquad (3)$$

where the mean value of r_g^2 is

$$\langle r_g^2\rangle = \frac{\int r_g^2 P\,dr_g}{\int P\,dr_g} \qquad (4)$$

In the Hermans–Overbeek approximation[10] $\langle r_g^2\rangle^{1/2}$ is taken to be the value of r_g that satisfies

$$\frac{\partial}{\partial r_g}(r_g P) = 0 \qquad (5)$$

Substituting eq 2 for the Gaussian distribution into eq 5 gives

$$\frac{\partial}{\partial \alpha_s}\left(\ln \alpha_s^3 - \frac{3}{2}\alpha_s^2 - \frac{\Delta F(\alpha_s)}{kT}\right) = 0 \qquad (6)$$

Flory[23] derived $\Delta F(\alpha_s)$ based on the Flory–Huggins theory for the entropy of mixing of solvent and polymer segments, which gives

$$\Delta F(\alpha_s) = f\alpha_s^{-3} \qquad (7)$$

Combined with eq 6, eq 7 yields

$$\alpha_s^5 - \alpha_s^3 = \frac{f}{kT} \qquad \text{Flory} \qquad (8)$$

The earlier treatment of coil expansion by Stigter[18] was essentially based on eq 8, with the function f derived from the interaction between long, rodlike segments.

If instead of the Gaussian distribution in eq 2 we use the Flory–Fisk distribution[1]

$$P(r_g)\,dr_g = C' r_g^6 \exp\left(-\frac{7}{2}\frac{r_g^2}{\langle r_g^2\rangle_0} - \frac{\Delta F}{kT}\right) dr_g \qquad (9)$$

then eqs 3, 5, and 7 lead to

$$\alpha_s^5 - \alpha_s^3 = \frac{3}{7}\frac{f}{kT} \qquad (10)$$

In a theory of heteropolymers[21,22] the equilibrium has been found as the maximum of the Flory–Fisk distribution[1] in eq 9 with respect to the coil density. This is equivalent to using $\partial P(r_g)/\partial r_g = 0$ instead of eq 5 and gives

$$\alpha_s^5 - \alpha_s^3 = \frac{1}{2}\frac{f}{kT} \qquad (11)$$

In perturbation approach the expansion factor α_s for the radius of gyration has been developed in powers of the intersegment interaction parameter z. In terms of this parameter the Flory theory, eq 8, becomes (ref 3, p 93)

$$\alpha_s^5 - \alpha_s^3 = 2.60z \qquad \text{Flory} \qquad (12)$$

On the other hand, for small z the result of a more rigorous perturbation treatment is

$$\alpha_s^5 - \alpha_s^3 = \frac{134}{105}z = 1.276z \qquad (13)$$

Equation 13 is an improvement over eq 12 (ref 3, p 93): intersegment interactions are about half as effective as assumed by Flory in eqs 8 and 12. A corresponding comparison of eqs 11 and 8 indicates that the heteropolymer theory[21,22] is a good approximation and it supports the use of the Flory–Fisk distribution[1] rather than the Gaussian distribution. We are interested in conformations not near Θ conditions—large expansions for polyelectrolytes, for example, for which perturbation theories are not applicable (compare ref 3, Figure III.4 on p 92). The α_s dependence in eq 7 follows from the pair interaction between chain segments or lattice sites, an assumption common to all theories of coil expansion. Therefore, the similar form of eqs 8 and 10–13 suggests that an important ingredient of, if not the key to, a successful theory is a good approximation for this pair interaction between chain segments.

5. Kinked Rod Model and Radius of Gyration.

Now we discuss how the electrostatic interactions are incorporated into this treatment. We model chains as random flights of segments that are locally rigid rods and are connected by universal joints. We call this the "kinked rod" model. The chain has elastic entropy that arises from the conformational statistics; we approximate this using the Flory–Fisk distribution[1] of eq 9. The contour length of each chain molecule is L. We account for intrachain interactions by assuming that pairs of chain segments interact as if they were disconnected rigid rods. For highly charged chains electrostatic repulsion prevents contacts between nonadjacent chain segments. Therefore, there is no separate term for the steric excluded volume of the chain since this is subsumed under the electrostatic repulsion. This electrostatic repulsion is treated in terms of an excluded volume around the chain defined by the effective chain diameter d_B discussed above. The rod/rod interaction part of the theory developed previously[18] predicts well the second virial coefficients of short DNA rods.[34] The second electrostatic contribution is the stiffening of the chain by the repulsion of adjacent and near-adjacent charges along the chain. Such repulsions determine the persistence length P of the chain.

We are thus assuming that chain interactions can be factored into "local" (elastic) and "nonlocal" (excluded volume) components, with the Flory–Fisk distribution[1] describing interactions among neighboring bonds along the chain and the rod interaction model describing the further reduction of conformations due to electrostatic excluded volume among segments further apart in the sequence. In the latter term, bond orientational correlations that arise from chain connectivity are neglected since those effects are already approximately accounted for in the elasticity term.

Our reference is the Θ state. In Θ solvents the radius of gyration of the coil without interactions is[43]

$$(r_g)_0 = \left(\frac{PL}{3}\right)^{1/2} \qquad (14)$$

where the subscript 0 refers to the reference state and the persistence length $P = P_{intr} + P_{elec}$ is the sum of the intrinsic persistence length of the uncharged chain, P_{intr}, and the electrostatic contribution, P_{elec}, which depends on the charge and the ionic strength. Considering the coil to be a uniformly filled sphere with volume V, we define the coil density ϱ as the ratio of the specific volume of the chain with (average physical) diameter d, $V_{chain} = (\pi/4)d^2L$, to the total volume within which the coil resides:

$$\varrho = V_{chain}/V \qquad (15)$$

Thus $\varrho = 1$ for the maximally compact chain. In the Θ state the chain density is given in terms of the reference state coil radius r_0 as

$$\varrho_0 = \frac{V_{chain}}{{}^4/_3\pi r_0^3} \qquad (16)$$

Thus the relation between the linear coil expansion factor α_s of eq 3 and the coil density is $\alpha_s^3 = \varrho_0/\varrho$. Since

the square radius of gyration of a uniform sphere is 3/5 times its radius squared, the coil radius in the Θ state follows from eq 14 with $r_0 = (r_g)_0(5/3)^{1/2}$.

The elastic free energy of deformation of a single coil with density ϱ is[1]

$$\frac{F_{elastic}}{kT} = \frac{7}{2}\left(\frac{\varrho_0}{\varrho}\right)^{2/3} + 2\ln\frac{\varrho}{\varrho_0} \tag{17}$$

Now we consider the intrachain excluded volume repulsions. We use an approach developed previously[18] and divide the charged chain into n rodlike segments, each of length $l = L/n$. We assume segments are distributed throughout the coil volume. In two different models, we first assume the rods have uniform concentration $c = n/V$ throughout the chain volume and then assume the rods have a Gaussian distribution, with highest concentration at the center (see Appendix A). In the virial expansion of the osmotic free energy $\Pi V = kTV(c + B_2c^2 + ...)$ of the segments the leading (van't Hoff) term is the ideal contribution of the solution of short rods, proportional to their concentration c, and the higher terms account for the interaction between the rods. The connectivity of the segments in the real chain eliminates the first term (translational entropy) but there is no reason to believe it affects the higher terms. Hence, we assume for the pair segment repulsion

$$\frac{F_{elec}}{kT} = VB_2c^2 \tag{18}$$

In this expression B_2 is the second virial coefficient between two rodlike segments of length l

$$B_2 = \frac{\pi}{4}l^2d_B \tag{19}$$

where d_B is the rod diameter. How should we choose this diameter? In the present treatment, we suppose it is an effective diameter identical to that which would arise from the pair repulsion between infinitely long charged rods.[27] The justification for neglecting end effects is that in the present model the rods are connected into a chain. Combining eqs 18 and 19 gives

$$\frac{F_{elec}}{kT} = \frac{\pi}{4}L^2d_B\frac{1}{V} = \frac{\pi}{4}\frac{L^2d_B}{V_{chain}}\varrho \tag{20}$$

The length l and the number n of segments cancel in the product $l^2c^2 = (L/n)^2(n/V)^2 = L^2/V^2$. This is the reason that F_{elec} in eq 20 does not depend on the details of the fictional subdivision of the chain molecule into segments.

As mentioned already, electrostatics plays two roles in the model. First, it contributes to the effective rod diameter, d_B. Second, it affects the persistence length P of the chain. We account for this latter effect through a dependence of $(r_g)_0$ in eq 14, and hence ϱ_0 in eq 16. In general, the charge effects on the persistence length and on the excluded volume statistics cannot be easily separated. Different ways of modeling these factors may lead to different predictions.[44] We use the approaches of Le Bret[17] and Fixman,[16] who treated the electrostatic part of the persistence length, P_{elec}, with the full Poisson–Boltzmann (PB) equation. Thus we have

$$P = P_{intr} + P_{elec} \tag{21}$$

where P_{intr} is the intrinsic persistence length of the (uncharged) chain.

Adding eqs 17 and 20 gives the free energy of a polyelectrolyte molecule of density ϱ

$$\frac{F_1}{kT} = \frac{F_{elastic}}{kT} + \frac{F_{elec}}{kT} = \frac{7}{2}\left(\frac{\varrho_0}{\varrho}\right)^{2/3} + 2\ln\frac{\varrho}{\varrho_0} + \frac{\pi}{4}\frac{L^2d_B}{V_{chain}}\varrho \tag{22}$$

The radius of gyration, r_g, can be readily obtained from the density ϱ:

$$r_g = (r_g)_0\left(\frac{\varrho_0}{\varrho}\right)^{1/3} \tag{23}$$

The root mean square r_g, which will be compared below with light scattering experiments, is given by

$$\langle r_g^2\rangle = \frac{\int_0^\infty r_g^2 e^{-F_1/kT}\,dr_g}{\int_0^\infty e^{-F_1/kT}\,dr_g} \tag{24}$$

In practice, these integrations are performed only over finite ranges, with limits chosen so that enlarging the range does not alter the integrals significantly.

The most probable density of the single coil, ϱ_s, is obtained by minimizing F_1 with respect to ϱ

$$\frac{\partial F_1}{\partial \varrho} = 0 \qquad \text{at } \varrho = \varrho_s \tag{25}$$

In some applications the coil properties at this most probable coil density are of interest.[21,22] We shall compare rms radii of gyration from eq 24 with values at $\varrho = \varrho_s$ from eq 25.

6. Second Virial Coefficient, Uniform Density Model

The model above describes the free energy for a single chain. We now consider the interactions between chains. We compare different models. First, we distinguish how the rod segments are distributed throughout the volume occupied by the chain. (i) In the uniform density model, we assume that the rod segments are distributed uniformly throughout the coil volume. (ii) In the Gaussian density model we assume the rod segments have the highest density at the center of the chain volume and that their density decreases radially according to a Gaussian distribution. Below we give details for the uniform density model. In Appendix A the treatment of the Gaussian model is summarized. Second, we model fluctuations at different levels of approximation. (1) Using the uniform density model, we assume that two approaching chains remain spherical at all separations, including those in which their center-of-mass separation is smaller than their radii. We compare two cases: (a) accounting only for the average (i.e., most probable) radius of each coil or (b) also accounting for the fluctuations in radii of the individual coils. We find that these models are indistinguishable, so the fluctuations are unimportant here. (2) We model the perturbations of one chain by another through mutual deformation into nonspherical shapes. We find that accounting for these mutual deformations gives the best agreement with experiments.

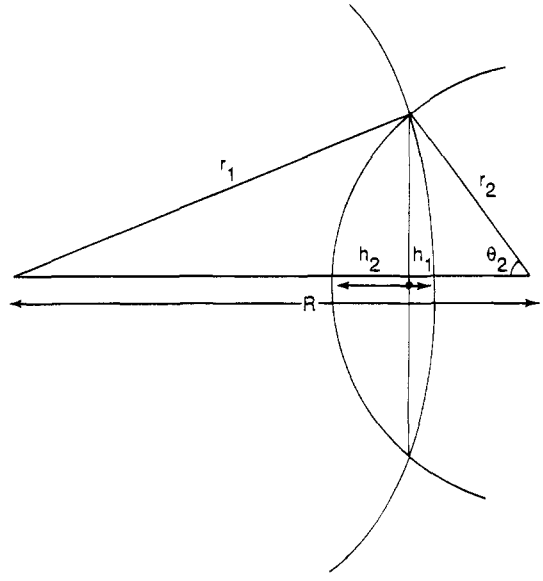

Figure 1. Overlapping spherical coils of uniform density.

The second virial coefficient of polymers with molecular weight M is defined as

$$A_2 = -\frac{N_{Av}}{2M^2}\int_0^\infty (e^{-w(R)/kT} - 1)(4\pi R^2)\, dR \qquad (26)$$

where $w(R)$ is the potential of mean force between two coils in the salt solution at distance R between their centers.[45] Physically, $w(R)$ is the integrated force, $-dw(R)/dR$, acting on coils as they move reversibly from infinite separation, where $w = 0$, to distance R. At each R the force is averaged with respect to all significant fluctuating variables such as coil size and shape. For example, the potential of mean force is an average over a degree of freedom, x:

$$e^{-w(R)/kT} = \frac{1}{x_2 - x_1}\int_{x_1}^{x_2} e^{-w(R,x)/kT}\, dx \qquad (27)$$

over the range x_1 to x_2. If we take the logarithm of both sides of eq 27 and then differentiate with respect to R, the result is

$$-\frac{dw(R)}{dR} = \frac{\int_{x_1}^{x_2} -\frac{\partial w(R,x)}{\partial R} e^{-w(R,x)/kT}\, dx}{\int_{x_1}^{x_2} e^{-w(R,x)/kT}\, dx} \qquad (28)$$

which shows that $-dw(R)/dR$ is the Boltzmann average of the fluctuating force $-\partial w(R,x)/\partial R$ between the two chains.

We now derive the pair potential between two coils with radii r_1 and r_2, respectively, and with a distance R between their centers. In the first model, we assume that interacting coils remain spherical and that their sizes fluctuate independently of each other. Deviations from spherical coil shape will be introduced later. The interaction potential is evaluated as the difference between the free energy of the two coils, F_2, at distances R and $R = \infty$:

$$w(R,r_1,r_2) = F_2(R,r_1,r_2) - F_2(R{=}\infty,r_1,r_2) \qquad (29)$$

If the radii of the two chains fluctuate independently, then the potential of mean force will be given by

$$e^{-w(R)/kT} = \frac{\int_a^b\int_a^b e^{-F_2(R,r_1,r_2)/kT}\, dr_1\, dr_2}{\int_a^b\int_a^b e^{-F_2(R=\infty,r_1,r_2)/kT}\, dr_1\, dr_2} \qquad (30)$$

From $w(R)$ obtained in this way, eq 26 can then be used to compute A_2.

It remains to specify the free energy of two interacting coils, $F_2(R,r_1,r_2)$. We assume this free energy has the same elastic and excluded volume components as that of a single coil. Computations with the charged porous sphere model of Hermans and Overbeek[10] have shown that the electrostatic interaction between nonoverlapping large coils is insignificant. Hence we set $F_2(R,r_1,r_2) = F_1(r_1) + F_1(r_2)$ for $R \geq r_1 + r_2$.

Before considering the free energy of overlapping coils, we describe the volume of the overlap region between two chains near in space. Figure 1 defines the geometric parameters for the overlap volume. From the two geometric equalities in Figure 1

$$R = r_1 - h_1 + r_2 \cos\theta_2 \qquad (31)$$

$$(r_2 \sin\theta_2)^2 = r_1^2 - (r_1 - h_1)^2 \qquad (32)$$

we eliminate the angle θ_2 and find

$$h_1 = r_1 - \frac{R}{2} + \frac{r_2^2 - r_1^2}{2R} \qquad (33)$$

Similarly

$$h_2 = r_2 - \frac{R}{2} + \frac{r_1^2 - r_2^2}{2R} \qquad (34)$$

Thus the overlapping volume, ΔV, of the two spheres will be

$$\Delta V = \frac{1}{3}\pi h_1^2(3r_1 - h_1) + \frac{1}{3}\pi h_2^2(3r_2 - h_2) \quad \text{for } |r_1 - r_2| < R < r_1 + r_2 \qquad (35)$$

For larger R there is no overlap at all

$$\Delta V = 0 \qquad \text{for } R > r_1 + r_2 \qquad (36)$$

and for smaller distances complete overlap gives

$$\Delta V = V_2 = \frac{4}{3}\pi r_2^3 \qquad \text{for } r_1 > r_2 \text{ and } R < r_1 - r_2 \qquad (37)$$

$$\Delta V = V_1 = \frac{4}{3}\pi r_1^3 \qquad \text{for } r_2 > r_1 \text{ and } R < r_2 - r_1 \qquad (38)$$

We now obtain the pair free energy, $F_2(R,r_1,r_2)$ from the single-chain conformational free energies, $F_1(r_1)$ and $F_1(r_2)$. The free energies of the single coils, $F_1(r_1)$ and $F_1(r_2)$, are given by eq 22, with the respective densities, $\varrho = \varrho_1$ and $\varrho = \varrho_2$, corresponding to r_1 and r_2. We assume in the pair free energy, $F_2(R,r_1,r_2)$, that the elastic free energies of the two chains take the same form but that the (electrostatic) excluded volume term changes in the overlap region. Since the density of each chain is assumed uniform in its own spherical volume, the overlapping fraction of chain i ($i = 1,2$) is $\Delta V/V_i$ and the nonoverlapping fraction is $1 - \Delta V/V_i$. These frac-

tions scale the lengths and volumes of the chains. Hence, in view of eq 22, the excluded volume contributions of the nonoverlapping parts of the two chains are $(\pi/4)(L^2d_B/V_{chain})\varrho_1(1 - \Delta V/V_1)$ and $(\pi/4)(L^2d_B/V_{chain})\varrho_2(1 - \Delta V/V_2)$. Similarly, the overlapping coil volume ΔV contains chain with length $L(\Delta V/V_1 + \Delta V/V_2)$, volume $V_{chain}(\Delta V/V_1 + \Delta V/V_2)$, and density $\varrho_1 + \varrho_2$ and, hence, contributes $(\pi/4)(L^2d_B/V_{chain})(\varrho_1 + \varrho_2)(\Delta V/V_1 + \Delta V/V_2)$. Adding all contributions, we find for the free energy of two interacting coils

$$\frac{F_2(R,r_1,r_2)}{kT} = \frac{7}{2}\left(\frac{\varrho_0}{\varrho_1}\right)^{2/3} + 2\ln\frac{\varrho_1}{\varrho_0} + \frac{7}{2}\left(\frac{\varrho_0}{\varrho_2}\right)^{2/3} + 2\ln\frac{\varrho_2}{\varrho_0} + \frac{\pi}{4}\frac{L^2d_B}{V_{chain}}\left[\left(1 + \frac{\Delta V}{V_2}\right)\varrho_1 + \left(1 + \frac{\Delta V}{V_1}\right)\varrho_2\right] \quad (39)$$

where ΔV is taken from eqs 35–38.

Within this uniform density model, we take two different approaches to computing the second virial coefficient. First, the independent size fluctuations of the two coils are taken into account by substituting eq 39 into eq 30 to obtain the potential of mean force $w(R)$. A_2 is then computed using eq 26. A second approach is to neglect the fluctuations. In the latter case we consider the interaction between spheres of equal size whose density $\varrho_1 = \varrho_2 = \varrho$ minimizes F_2 in eq 39 (i.e., $\partial F_2/\partial\varrho = 0$) for each value of R. As shown below, both methods give essentially the same results for A_2.

7. Chain Deformability Improves A_2

In the models above, we have made the traditional assumption that two chains retain their spherical shapes as they approach and overlap. However, there is no particular reason to believe that chains will remain spherical when they overlap. When two polyelectrolyte molecules approach each other, the coils may flatten to reduce their overlap. We now consider a model in which the chains have a *shape* degree of freedom in addition to the *size* degree of freedom considered above. In particular, the chains may flatten as they approach so that there will be decreased repulsion in the smaller overlap volume, but there will also be a counteracting loss of elastic entropy. The net result can be a lower free energy than in chains with only a size degree of freedom. Here we investigate such effects for two coils of uniform density and the same volume. Chains of constant volume can deform from spherical shapes into ellipsoids having symmetry around their center-to-center axis. The extent of deformation is represented by the factor α, where $2\alpha r$ is the length of the rotation axis of the ellipsoid and $2r/\alpha^{1/2}$ is the length of the other two axes. We consider oblate ellipsoids, $\alpha < 1$, and prolate ellipsoids, $\alpha > 1$. The two coils may deform differently, measured by α_1 and α_2. According to the theory of rubber elasticity, a uniform deformation in one direction, at constant volume, raises the free energy per coil by[46,45]

$$\Delta F = \frac{kT}{2}\left(\alpha_i^2 + \frac{2}{\alpha_i} - 3\right) \quad (40)$$

In Appendix B we derive the overlap volume ΔV as a function of R, r, α_1, and α_2. The excluded volume effect is the same as in eq 39, with $V_1 = V_2 = V$ and $\varrho_1 = \varrho_2 = \varrho$. Collecting results, we find for the free energy of the interacting coils

$$\frac{F_2(R,\alpha_1,\alpha_2)}{kT} = 7\left(\frac{\varrho_0}{\varrho}\right)^{2/3} + 4\ln\frac{\varrho}{\varrho_0} + \frac{\pi}{2}\frac{L^2d_B}{V_{chain}}\left(1 + \frac{\Delta V}{V}\right)\varrho + \frac{1}{2}\left(\alpha_1^2 + \alpha_2^2 + \frac{2}{\alpha_1} + \frac{2}{\alpha_2} - 6\right) \quad (41)$$

Similar to eq 30, the shape fluctuations in $w(R)$ may be averaged using

$$e^{-w(R)/kT} = \frac{\int_a^b\int_a^b e^{-F_2(R,\alpha_1,\alpha_2)/kT}\,d\alpha_1\,d\alpha_2}{\int_a^b\int_a^b e^{-F_2(R=\infty,\alpha_1,\alpha_2)/kT}\,d\alpha_1\,d\alpha_2} \quad (42)$$

which, with eq 26, yields A_2.

For simplicity, we have derived ΔV in Appendix B only for $\alpha_1 < \alpha_2$, which is fully general since the two coils are equivalent. Hence we can replace $\int_a^b d\alpha_2\int_a^b d\alpha_1$ in eq 42 with $\int_a^b d\alpha_2\int_a^{\alpha_2} d\alpha_1$.

We have treated only conformations for which the line connecting the coil centers is an axis of rotational symmetry, omitting all other possible relative orientations of the two ellipsoids. Practical computer limitations prevent us from accounting for all such orientations, which would be required to obtain the full potential of mean force. Hence eq 42 should be regarded as only an approximation for the effect of coil shape on A_2. Averaging of the interaction between oblate ellipsoids ($\alpha < 1$) was computed from eq 42 with the integration limits $\int_{0.1}^1 d\alpha_2\int_{0.1}^{\alpha_2} d\alpha_1$. For prolate–prolate coil interactions we used $\int_1^4 d\alpha_2\int_1^{\alpha_2} d\alpha_1$, and for prolate–oblate coil interactions $\int_1^4 d\alpha_2\int_{0.1}^1 d\alpha_1$. We compare the results for A_2 with those that follow from the simultaneous minimization of $F_2(R,\varrho,\alpha_1,\alpha_2)$ with respect to ϱ, α_1, and α_2.

8. Applications to T7 DNA, to Col E1 DNA, and to Poly(styrene sulfonate)s

In this section, we compare calculations of the model with experiments. We find that increasing salt shields charge repulsions, leading to chains with smaller radii and reduced interchain repulsions. Figure 2 shows the theoretical and experimental radius of gyration of DNA from the T7 virus, a high molecular weight DNA with 39 936 base pairs.[47] The DNA parameters are taken to be the same as used elsewhere:[34] the hydrodynamic diameter is $d = 24$ Å, the fixed charge density is based on 0.73 e per phosphate, and the contour length is 3.37 Å per base pair. We take the effective diameter d_B, reproduced in Table 1, from the same paper. Table 3 shows the persistence length P as a function of NaCl concentration, as interpolated from the tables of Le Bret,[17] using $P_{intr} = 400$ Å. As expected, P increases with decreasing salt concentrations. The data show that the most probable coil density (from eqs 22 and 25 for the uniform density coil model) is always lower than the density in the reference state ϱ_0, as expected for coils with repulsive intrachain interactions. The most probable radius of gyration corresponding to these ϱ values increases markedly with decreasing NaCl concentration. The data shown in parentheses in Table 3 are the results for r_g for the Gaussian density model obtained by minimization of F_1 in eq A7 with respect to ϱ. On average, radii from the Gaussian density model are 0.5% higher than for the uniform density model, an insignificant difference.

Figure 2 shows that the radii r_g from the uniform density model predict well the experiments of Sobel and

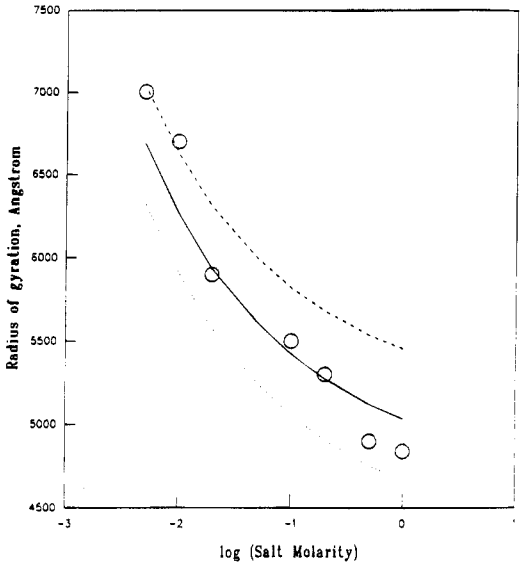

Figure 2. Radius of gyration of T7 DNA coil as a function of NaCl concentration. Solid curve: Uniform density coil, rms results from eq 24, P_{intr} = 400 Å. Dotted curve: Uniform density coil, most probable results from eq 25, P_{intr} = 400 Å. Dashed curve: Gaussian density coil, rms results from eq 24, P_{intr} = 500 Å. Circles: Experiments by Sobel and Harpst.[48]

Table 3. Data on T7 DNA

M_{NaCl}	P, Å	$10^5\varrho_0$	$10^5\varrho$	r_g,[a] Å
1	461	2.59	2.39	4670 (4687)
0.5	470	2.51	2.26	4754 (4772)
0.2	484	2.40	2.06	4909 (4929)
0.1	496	2.32	1.88	5058 (5082)
0.05	511	2.22	1.68	5251 (5278)
0.02	536	2.06	1.40	5578 (5609)
0.01	568	1.89	1.18	5911 (5947)
0.005	614	1.68	0.96	6330 (6370)

[a] For uniform density model, in parentheses for Gaussian density.

Harpst.[48] Also shown in Figure 2 are two curves for the rms radius of gyration, calculated with eqs 22 and 24 and assuming P_{intr} = 400 and 500 Å for the intrinsic persistence length. P_{intr} = 400 Å gives the best agreement with experiments. Consistent with this, in 0.002–1 M NaCl solutions, using essentially the same model and theory as above, intrinsic viscosity calculations of T7 DNA with P_{intr} = 425 Å showed excellent agreement[19] with experiments by Rosenberg and Studier.[49] The predicted DNA coil sizes in NaCl solutions appear to be in good agreement with experiments.

Figure 3 shows theory and experiment for the second virial coefficients of T7 DNA. It shows there is little difference between the uniform and Gaussian distribution models and that fluctuations contribute insignificantly. But A_2 is significantly reduced if the coil deformation is taken into account.

Borochov et al.[50] reported light scattering results of r_g and A_2 for plasmid Col E1 DNA which consists of 6594 ± 20 base pairs. In Figure 4 r_g is compared with the rms radius of gyration from eq 24. The solid curve, with P_{intr} = 400 Å, agrees well with the experiments except at high salt concentrations. For A_2 the comparison in Figure 5 shows also reasonable agreement between experiment and theory.

We have also applied the theory to sodium poly(styrenesulfonate) (PSS) in aqueous NaCl solutions. We assume a contour length of 2.49 Å per monomer and a uniform surface charge corresponding to one electronic charge per monomer. Lacking more accurate data, we

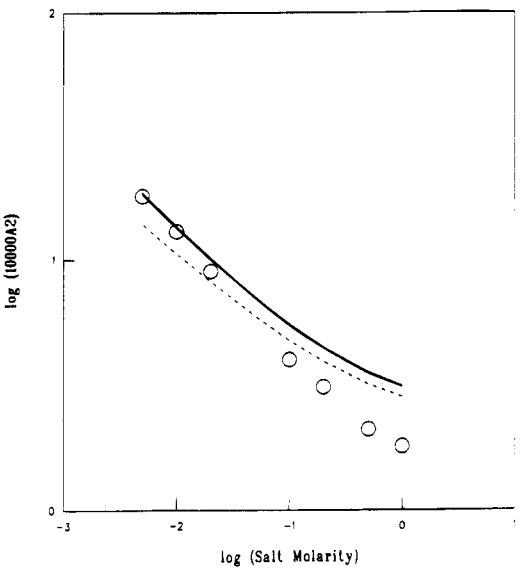

Figure 3. Second virial coefficient A_2 of T7 DNA versus NaCl concentration. Solid curve: Spherical coils, density uniform or Gaussian, mean force or most probable interaction potential, P_{intr} = 400 Å. Dashed curve: Uniform density model, ellipsoidal deformation, most probable interaction potential, P_{intr} = 400 Å. Dotted curve: Same as dashed curve, but with P_{intr} = 500 Å. Circles: Experiments by Sobel and Harpst.[48]

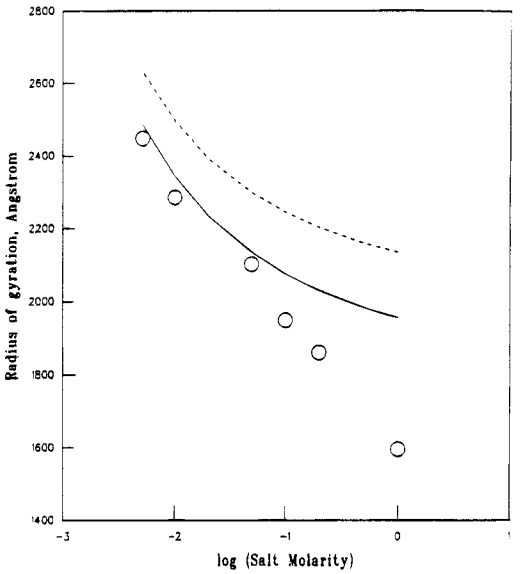

Figure 4. Radius of gyration of Col E1 DNA coil as a function of NaCl concentration. Solid curve: Uniform density coil, rms results from eq 24, P_{intr} = 400 Å. Dashed curve: Gaussian density coil, rms results from eq 24, P_{intr} = 500 Å. Circles: Experiments by Borochov et al.[50]

base the diameter of the cylindrical chain, d = 10.55 Å, on the molar volume of methylstyrene, 131 mL/mol. To determine how critical this choice is, we also use d = 11.5 Å for the chain diameter. Table 4 shows the persistence length, based on an intrinsic persistence length of five monomers in the chain[43] and an electrostatic contribution obtained with the tables of Le Bret[17] and on the effective diameter of the PSS chain as a function of the NaCl concentration evaluated according to Stigter.[27] The theory is compared with experiments by Takahashi et al.[51] and by Borochov and Eisenberg.[7]

Figures 6–8 show radii of gyration for PSS as functions of molecular weight and NaCl concentration. There is good agreement with experiments. We agree with an earlier assessment[18] that the high PSS concentrations used in the experiments may be the cause of

Table 4. Data on Sodium Poly(styrenesulfonate)

M_{NaCl}	P,[a] Å	d_B,[a] Å
0.5	27 (30)	21.1 (22.0)
0.2	32 (36)	30.4 (31.4)
0.1	37.5 (42.5)	41.6 (42.7)
0.05	44.5 (50.5)	58.4 (59.6)
0.02	57 (65.5)	94.1 (95.4)
0.01	76.5 (88.5)	136.8 (138.4)
0.005	104 (122)	200.7 (202.5)

[a] Based on chain diameter d = 10.55 Å, in parentheses on d = 11.5 Å.

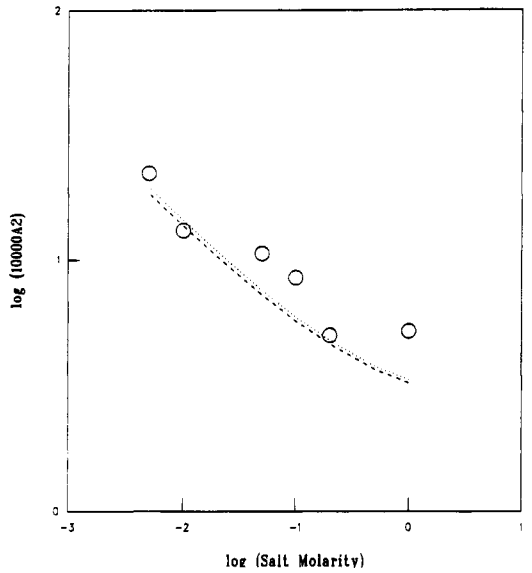

Figure 5. Second virial coefficient A_2 of Col E1 DNA versus NaCl concentration. Dashed curve: Uniform density model, ellipsoidal deformation, most probable interaction potential, P_{intr} = 400 Å. Dotted curve: Same as dashed curve, but with P_{intr} = 500 Å. Circles: Experiments by Borochov et al.[50]

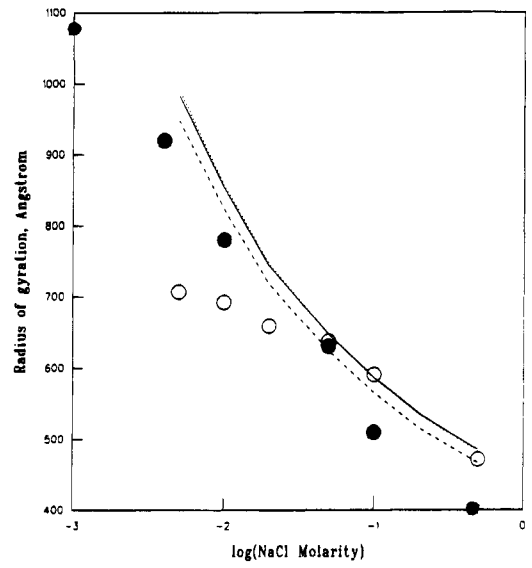

Figure 6. Radius of gyration of sodium poly(styrenesulfonate), M = 1 000 000, as a function of NaCl concentration. Computations for uniform density model. Solid curve: Rms results, chain diameter 10.55 Å. Dashed curve: Most probable values, chain diameter 10.55 Å. Dotted curve: Most probable values, chain diameter 11.5 Å. Open circles: Experiments by Takahashi et al.[51] Solid circles: Experiments by Borochov and Eisenberg.[7]

some discrepancies with the theory. Figures 6–8 show that effects of fluctuations are small and that chain diameters 10.5 and 11.5 Å give essentially the same results. We also find that the Gaussian and uniform

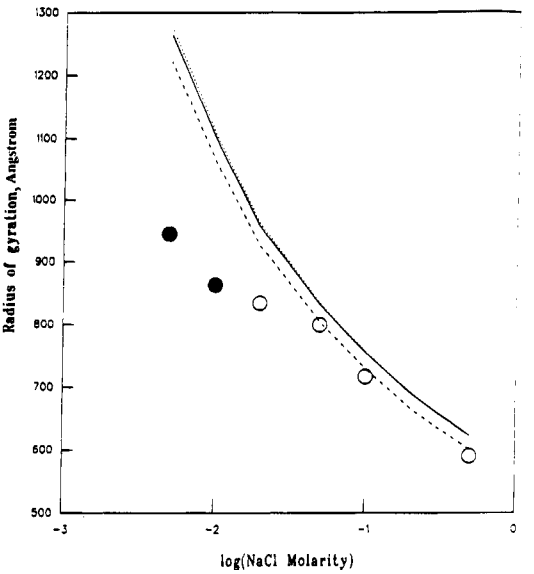

Figure 7. Radius of gyration of sodium poly(styrenesulfonate), M = 1 550 000, as a function of NaCl concentration. Computations for uniform density model. Solid curve: Rms results, chain diameter 10.55 Å. Dashed curve: Most probable values, chain diameter 10.55 Å. Dotted curve: Most probable values, chain diameter 11.5 Å. Circles: Experiments by Takahashi et al.[51] Solid circles: Coil overlap in all light scattering solutions.

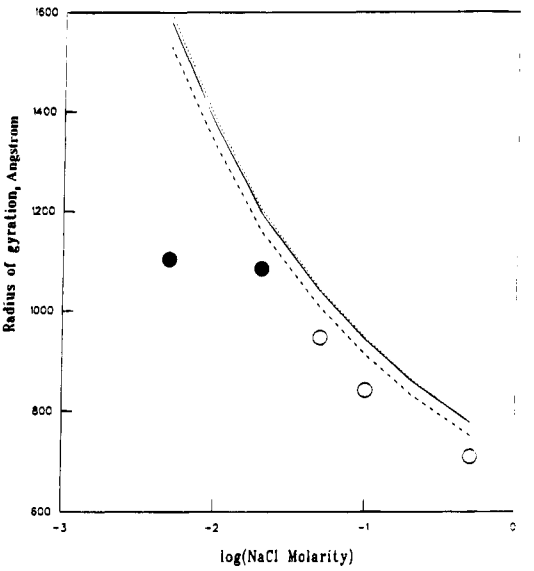

Figure 8. Same as Figure 7, for M = 2 280 000.

density models give nearly the same results (not shown). These points are confirmed in Figures 9–11.

Figure 6 also shows recent results reported by Borochov and Eisenberg[7] for NaPPS of $M = (0.98 \pm 0.026) \times 10^6$. Their light scattering experiments were carried out down to polymer concentrations about an order of magnitude lower than by Takahashi et al.[51] This explains the higher r_g values in the more dilute salt solutions.

We now compare in Figures 9–11 theory with experiments for the second virial coefficients. Here the experiments confirm the predicted near independence of A_2 on polymer molecular weight for this system. The theory for A_2 (dashed curves in Figures 9–11) is in reasonable agreement with the experiments by Takahashi et al.,[51] while the recent results for A_2 by Borochov and Eisenberg[7] in Figure 9 are considerably lower, presumably because of the lower polymer concentrations

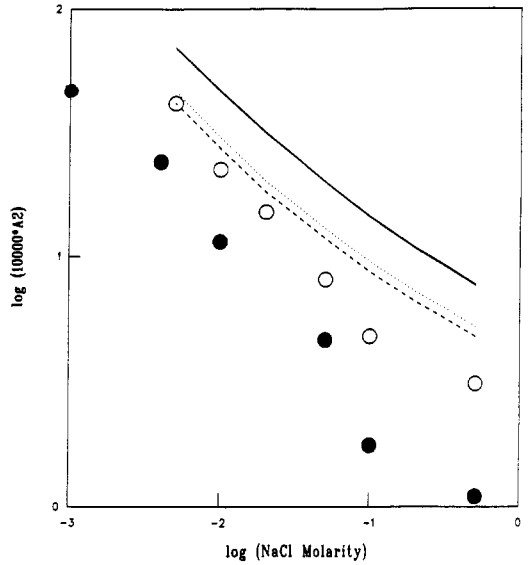

Figure 9. Second virial coefficient A_2 of sodium poly(styrenesulfonate), $M = 1\,000\,000$, as a function of NaCl concentration. Solid curve: Spherical coils, density uniform or Gaussian, mean force or most probable interaction potential, chain diameter 10.55 Å. Dashed curve: Uniform density model, ellipsoidal deformation, most probable interaction potential, chain diameter 10.55 Å. Dotted curve: Same as dashed curve, but with chain diameter 11.5 Å. Open circles: Experiments by Takahashi et al.[51] Solid circles: Experiments by Borochov and Eisenberg.[7]

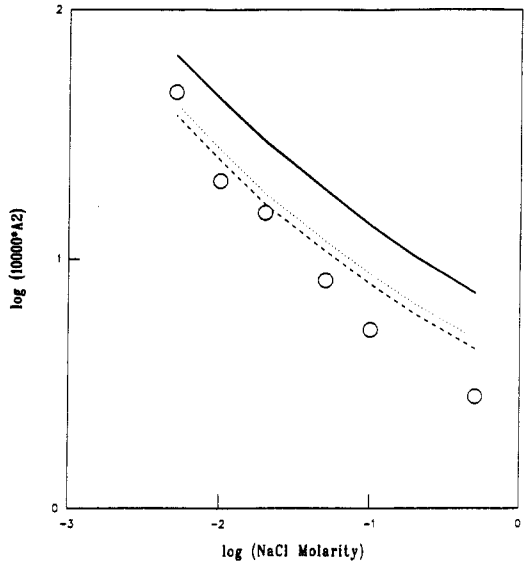

Figure 10. Second virial coefficient A_2 of sodium poly(styrenesulfonate), $M = 1\,550\,000$, as a function of NaCl concentration. Solid curve: Spherical coils, density uniform or Gaussian, mean force or most probable interaction potential, chain diameter 10.55 Å. Dashed curve: Uniform density model, ellipsoidal deformation, most probable interaction potential, chain diameter 10.55 Å. Dotted curve: Same as dashed curve, but with chain diameter 11.5 Å. Circles: Experiments by Takahashi et al.[51]

used in the light scattering experiments, as mentioned above.

In Figures 3 and 9–11 the experimental data on A_2 show a steeper dependence on the ionic strength than the theoretical curves. There may be several reasons for this discrepancy. It might be due, at least partly, to experimental error. Experimentally A_2 was determined from the limiting slope of a light scattering plot of c_p/R_θ versus c_p. These plots, as shown in Figure 3 of Takahashi et al.,[51] are not linear but curve upward in

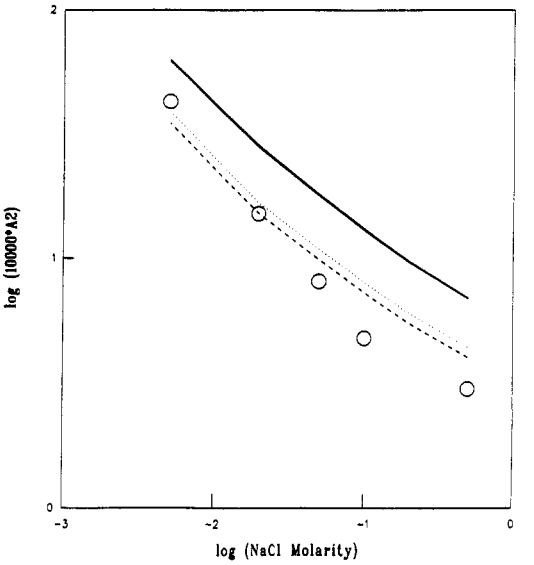

Figure 11. Same as Figure 10, for $M = 2\,280\,000$.

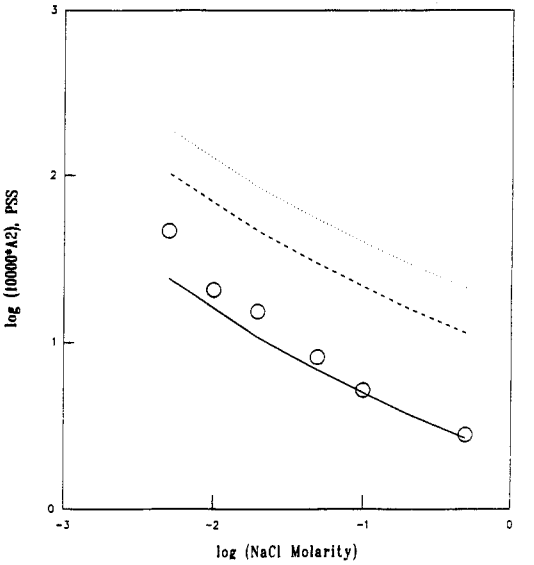

Figure 12. Effects of coil shape on second virial coefficient A_2 of sodium poly(styrenesulfonate), $M = 1\,550\,000$, as a function of NaCl concentration. Chain diameter 10.55 Å, uniform density model, averaging of shape effects with eq 52. Solid curve: Oblate–oblate interactions. Dashed curve: Oblate–prolate interactions. Dotted curve: Prolate–prolate interactions. Circles: Experiments by Takahashi et al.[51]

the experimental range of polymer concentrations c_p. The curvature is typical for significant contributions of a positive third virial coefficient, consistent with the coil overlap discussed in connection with Figures 6–8. The curvature of the plot makes the determination of A_2 inaccurate, and the reported A_2 values are probably too high, particularly in solutions of low ionic strength. Moreover, in solutions of higher ionic strength the Poisson–Boltzmann approach becomes increasingly inaccurate and, because electrostatic shielding allows closer approach between chain segments, our neglect of van der Waals attraction may be a problem. Including such attraction would increase the calculated change of A_2 with ionic strength.

Figure 12 shows the effects of the shape deformations on A_2 of the chains for the $M = 1\,550\,000$ fraction of PSS. Computer limitations restricted us to considering only a few simple coil shape fluctuations using eq 52: for interacting oblate chains, for prolate chains, and for the mixed case of oblate coils interacting with prolate

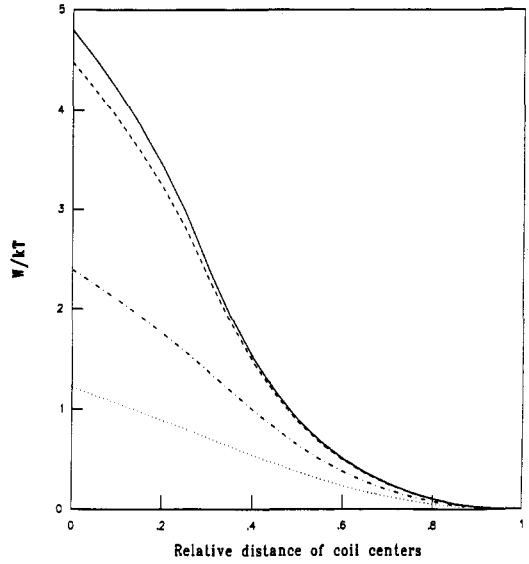

Figure 13. Most probable pair potential w between overlapping coils as a function of relative distance between coil centers, $R/2r_s$. Solid curve: sodium poly(styrenesulfonate), M = 1 550 000, in 0.1 M NaCl. Dashed curve: sodium poly(styrenesulfonate), M = 1 550 000, in 0.005 M NaCl. Dashed–dotted curve: T7 DNA in 0.005 M NaCl. Dotted curve: T7 DNA in 0.1 M NaCl.

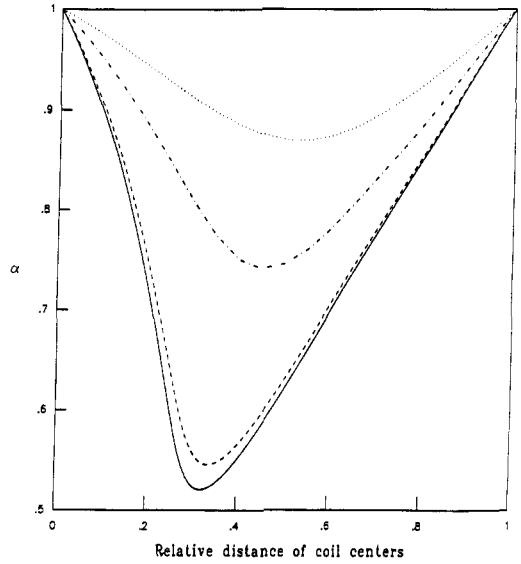

Figure 14. Deformation parameter α of overlapping coils as a function of relative distance between coil centers, $R/2r_s$, from free energy minimization. Solid curve: sodium poly(styrenesulfonate), M = 1 550 000, in 0.1 M NaCl. Dashed curve: sodium poly(styrenesulfonate), M = 1 550 000, in 0.005 M NaCl. Dashed–dotted curve: T7 DNA in 0.005 M NaCl. Dotted curve: T7 DNA in 0.1 M NaCl.

coils. Theory comes into closest agreement with the data if we assume that the two chains both have oblate shapes upon deformation. Since in no case could we average the full set of interacting coil shapes and orientations, these computations only can approximate the true potentials of mean force. It is clear that oblate shapes that reduce chain overlap (solid line in Figure 12) lower A_2 considerably. On the other hand, the increased overlap between prolate coils increases A_2 compared with the spherical coil results in Figure 10. The main conclusion from Figure 12 is that coil shape is an important factor in determining A_2, but that it is uncertain how close the free energy minimization values of A_2 are to rigorous mean force potential results. This caveat holds also for the work of Grosberg and Kuznetsov,[52] who addressed the chain distribution of overlapping, uncharged polymers in poor solvents.

Figure 13 shows how the predicted repulsion increases as chain separation decreases. The repulsion is weakened by salt. It shows that the repulsion between PSS chains is stronger than between the more open T7 DNA molecules. Figure 14 shows that the deformation from spherical shape is greatest for intermediate degrees of overlap. When there is no overlap, the chains have spherical symmetry, and when there is complete overlap, both chains centered at the same point, there is also spherical symmetry. Consistent with Figure 13, chains with the strongest repulsions induce the greatest deformations.

9. Conclusions

We have developed a simple theory for conformational changes in polyelectrolytes and for the pairwise interactions between two polyelectrolyte chains. The free energy is comprised of two terms: an elastic term based on the Flory–Fisk distribution function and an electrostatic (excluded volume) term based on Stigter's treatment of charged rods. We have found that the model is quite insensitive to the main uncertainties in the model: it is not sensitive to the chain diameter or to the distribution of segments throughout the coil—whether it is uniform or Gaussian. We have found that the most probable radius is not much smaller than the rms value in which fluctuations are taken into account and that coil size fluctuations do not affect A_2. We find that there are significant correlations between the conformations of two chains as they approach each other: a mutual deformation into ellipsoids allows the chains to avoid unfavorable repulsions. For DNA and for poly(styrenesulfonate) the model predicts the radii of gyration and second virial coefficients nearly to within experimental error.

Appendix A

For nonuniform density distributions of the coil the generalization of eq 18 for the intrachain interactions is

$$\frac{F_{\text{elec}}}{kT} = \int B_2 c^2 \, dV \tag{A1}$$

We consider a Gaussian density distribution with spherical symmetry

$$c = a \exp\left(\frac{-5}{2}\frac{r^2}{r_u^2}\right) \tag{A2}$$

where r_u is the radius of the uniform coil with the same radius of gyration. For a single chain, the conservation of chain segments

$$\int c \, dV = n = L/l \tag{A3}$$

gives

$$a = \left(\frac{5}{2\pi}\right)^{3/2} \frac{L}{l r_u^3} \tag{A4}$$

With eqs A2 and A4 for c and eq 19 for B_2, integration of eq A1 yields

$$\frac{F_{elec}}{kT} = \frac{5}{32}\left(\frac{5}{\pi}\right)^{1/2}\frac{L^2 d_B}{r_u^3} \quad \text{(A5)}$$

For comparison, if we introduce volume V and density ϱ of the equivalent uniform coil with

$$V = \frac{4}{3}\pi r_u^3 = \frac{V_{chain}}{\varrho} \quad \text{(A6)}$$

then at the same density ϱ, eq A5 gives a value for F_{el} that is 5.1% higher than the uniform model, eq 20. The free energy of the Gaussian coil is obtained using eqs A5 and A6 and is added to the elastic free energy of the chain (eq 17)

$$\frac{F_1}{kT} = \frac{7}{2}\left(\frac{\varrho_0}{\varrho}\right)^{2/3} + 2\ln\frac{\varrho}{\varrho_0} + \frac{5(5\pi)^{1/2}}{24}\frac{L^2 d_B}{V_{chain}}\varrho \quad \text{(A7)}$$

Flory and Krigbaum[53] have evaluated the interaction between two Gaussian coils of the same size. Their pair potential was used later by Orofino and Flory[2] and is discussed also by Yamakawa.[3] From this Flory–Krigbaum treatment,[53] the overlap ratio of two Gaussian coils at distance R is given by

$$\frac{\Delta V}{V} = e^{-5R^2/4r_u^2} \quad \text{(A8)}$$

This ratio plays the same role as the overlap ratio $\Delta V/V_1 = \Delta V/V_2$ of two uniform coils of the same size in eq 39. Hence, with the replacements $r_u = r_1 = r_2$ and $\varrho = \varrho_0(r_0/r_u)^3$, we now have (instead of eq 39)

$$\frac{F_2(R,\varrho)}{kT} = 7\left(\frac{\varrho_0}{\varrho}\right)^{2/3} + 4\ln\frac{\varrho}{\varrho_0} + \left(1 + \frac{\Delta V}{V}\right)\frac{5(5\pi)^{1/2}}{12}\frac{L^2 d_B}{V_{chain}}\varrho \quad \text{(A9)}$$

After minimizing $F_2(R,\varrho)$ with respect to ϱ for each R, the pair potential is

$$w(R) = F_2(R) - F_2(R=\infty) \quad \text{(A10)}$$

which is then used to evaluate A_2 by integration in eq 26.

Appendix B

We evaluate the overlap volume, ΔV, between two ellipsoids with volume $(4/3)\pi r^3$ and with rotational symmetry around the x axis. The centers are at $x_1 = 0$ for ellipsoid 1 and at x_2 for ellipsoid 2. The respective axes are $2r\alpha_1$ and $2r\alpha_2$ along the x axis and $2r/\alpha_1^{1/2}$ and $2r/\alpha_2^{1/2}$ in the y and z directions. Figure B1 shows part of the xy cross-sections which are given by the eqs

$$\frac{x_1^2}{\alpha_1^2 r^2} + \frac{\alpha_1 y_1^2}{r^2} = 1 \qquad \text{for ellipsoid 1} \quad \text{(B1)}$$

$$\frac{(x_2 - R)^2}{\alpha_2^2 r^2} + \frac{\alpha_2 y_2^2}{r^2} = 1 \qquad \text{for ellipsoid 2} \quad \text{(B2)}$$

We consider only cases for which $\alpha_2 > \alpha_1$.

The common points of the two elliptical cross-sections are given by $x_1 = x_2 = x$ and $y_1 = y_2 = y$. Eliminating y, this gives

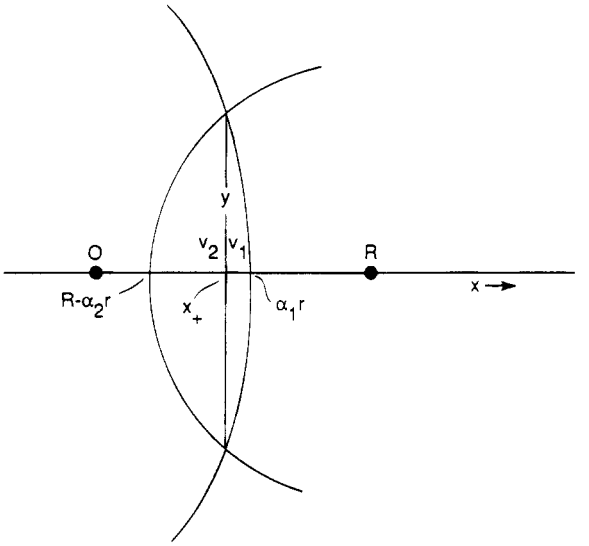

Figure B1. Cross-section of two overlapping ellipsoidal coils with distance R between centers, overlap volume $v_1 + v_2$.

$$(\alpha_2^3 - \alpha_1^3)x^2 + 2R\alpha_1^3 x - \alpha_1^3 R^2 - r^2(\alpha_1^2\alpha_2^3 - \alpha_1^3\alpha_2^2) = 0 \quad \text{(B3)}$$

with the solutions

$$x_\pm = [-R\alpha_1^3 \pm \alpha_1\alpha_2(R^2\alpha_1\alpha_2 + r^2(\alpha_2 - \alpha_1)^2(\alpha_1^2 + \alpha_1\alpha_2 + \alpha_2^2))^{1/2}]/(\alpha_2^3 - \alpha_1^3) \quad \text{(B4)}$$

The roots x_+ and x_- are always real, on the positive and negative x axis, respectively. However, the corresponding y values following from eq B1

$$y^2 = \frac{r^2}{\alpha_1} - \frac{x^2}{\alpha_1^3} \quad \text{(B5)}$$

are real only if x satisfies

$$-\frac{r}{\alpha_1} < x < \frac{r}{\alpha_1} \quad \text{(B6)}$$

as expected from geometry. The overlap volume of the ellipsoids depends on R, r, α_1, and α_2. There is no overlap

$$\Delta V = 0 \qquad \text{for } R > r(\alpha_1 + \alpha_2) \quad \text{(B7)}$$

For $r(\alpha_2 - \alpha_1) < R < r(\alpha_1 + \alpha_2)$ the point (x_+,y_+) is real, but (x_-,y_-) is complex. The overlap, illustrated for this case in Figure B1, is

$$\Delta V = v_1 + v_2 \quad \text{(B8)}$$

$$v_1 = \int_{x_-}^{\alpha_1 r} \pi y_1^2\, dx_1 = \pi\int_{x_+}^{\alpha_1 r}\left(\frac{r^2}{\alpha_1} - \frac{x_1^2}{\alpha_1^3}\right)dx_1 = \frac{2}{3}\pi r^3\left(1 - \frac{3}{2}\frac{x_+}{\alpha_1 r} + \frac{1}{2}\frac{x_+^3}{\alpha_1^3 r^3}\right) \quad \text{(B9)}$$

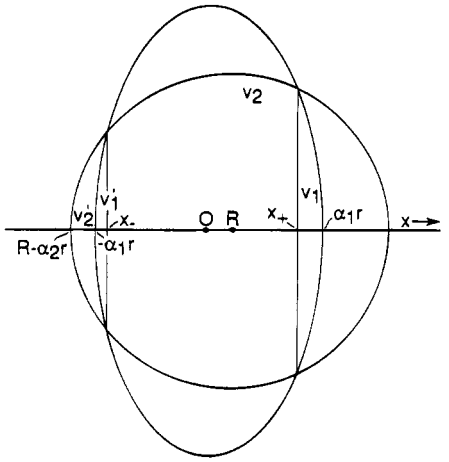

Figure B2. Cross-section of two overlapping ellipsoidal coils with distance R between centers, overlap volume $v_1 + v_2 + v_1' - v_2'$.

$$v_2 = \int_{R-\alpha_2 r}^{x_-} \pi {y_2}^2 \, dx_2 = \pi \int_{R-\alpha_2 r}^{x_+} \left(\frac{r^2}{\alpha_2} - \frac{(x_2 - R)^2}{{\alpha_2}^3} \right) dx_2 = \frac{2}{3}\pi r^3 \left(1 - \frac{3}{2}\frac{R - x_+}{\alpha_2 r} + \frac{1}{2}\frac{(R - x_+)^3}{{\alpha_2}^3 r^3} \right) \quad \text{(B10)}$$

Finally, for $0 < R < r(\alpha_2 - \alpha_1)$ the points (x_+, y_+) and (x_-, y_-) are both real, as illustrated in Figure B2. In this case eq B8 is too high by the volume $v_2' - v_1'$, so that we now have

$$\Delta V = v_1 + v_2 + v_1' - v_2' \quad \text{(B11)}$$

with v_1 and v_2 given by eqs B9 and B10 and

$$v_1' = \int_{-\alpha_1 r}^{x_-} \pi {y_1}^2 \, dx_1 = \frac{2}{3}\pi r^3 \left(1 + \frac{3}{2}\frac{x_-}{\alpha_1 r} - \frac{1}{2}\frac{{x_-}^3}{{\alpha_1}^3 r^3} \right) \quad \text{(B12)}$$

$$v_2' = \int_{R-\alpha_2 r}^{x_-} \pi {y_2}^2 \, dx_2 = \frac{2}{3}\pi r^3 \left(1 - \frac{3}{2}\frac{R - x_-}{\alpha_2 r} + \frac{1}{2}\frac{(R - x_-)^3}{{\alpha_2}^3 r^3} \right) \quad \text{(B13)}$$

References and Notes

(1) Flory, P. J.; Fisk, S. *J. Chem. Phys.* **1966**, *44*, 2243.
(2) Orofino, T. A.; Flory, P. J. *J. Phys. Chem.* **1959**, *63*, 283.
(3) Yamakawa, H. *Modern Theory of Polymer Solutions*; Harper and Row: New York, 1971.
(4) Fujita, H. *Polymer Solutions*; Elsevier: New York, 1990.
(5) des Cloizeaux, J.; Jannink, G. *Polymer Solutions, Their Modelling and Structure*; Clarendon Press: Oxford, 1990.
(6) De Gennes, P. G.; Pincus, P.; Velasco, R. M. *J. Phys. (Paris)* **1976**, *37*, 1461.
(7) Borochov, N.; Eisenberg, H. *Macromolecules* **1994**, *27*, 1440.
(8) Stevens, M. J.; Kremer, K. *Macromolecules* **1993**, *26*, 4717.
(9) Stevens, M. J.; Kremer, K. *Phys. Rev. Lett.* **1993**, *71*, 2228.
(10) Hermans, J. J.; Overbeek, J. Th. G. *Recl. Trav. Chim. Pays-Bas* **1948**, *67*, 761.
(11) Alfrey, T., Jr.; Berg, P. W.; Morawetz, H. *J. Polym. Sci.* **1951**, *7*, 1951.
(12) Fuoss, R. M.; Katchalsky, A.; Lifson, S. *Proc. Natl. Acad. Sci. U.S.A.* **1951**, *37*, 579.
(13) Odijk, T. *J. Polym. Sci., Polym. Phys. Ed.* **1977**, *15*, 477.
(14) Odijk, T.; Houwaart, A. C. *J. Polym. Sci., Polym. Phys. Ed.* **1978**, *16*, 627.
(15) Skolnick, J.; Fixman, M. *Macromolecules* **1977**, *10*, 944.
(16) Fixman, M. *J. Chem. Phys.* **1982**, *76*, 6346.
(17) Le Bret, M. *C. R. Seances Acad. Sci., Ser. 2* **1981**, *292*, 291; *J. Chem. Phys.* **1982**, *76*, 6243.
(18) Stigter, D. *Macromolecules* **1982**, *15*, 635.
(19) Stigter, D. *Macromolecules* **1985**, *18*, 1619.
(20) Sanchez, I. C. *Macromolecules* **1979**, *12*, 980.
(21) Dill, K. A. *Biochemistry* **1985**, *24*, 1501.
(22) Dill, K. A.; Alonso, D. O. V.; Hutchinson, K. *Biochemistry* **1989**, *28*, 5439.
(23) Flory, P. J. *Principles of Polymer Chemistry*; Cornell University Press: Ithaca, NY, 1953.
(24) Birshtein, T. M.; Pryamitsyn, V. A. *Macromolecules* **1991**, *24*, 1554.
(25) Gobush, W.; Solc, K.; Stockmayer, W. H. *J. Chem. Phys.* **1974**, *60*, 12.
(26) Fixman, M.; Skolnick, J. *Macromolecules* **1978**, *11*, 863.
(27) Stigter, D. *Biopolymers* **1977**, *16*, 1435.
(28) Schellman, J. A.; Stigter, D. *Biopolymers* **1977**, *16*, 1415.
(29) Vologodskii, A. V.; Cozzarelli, N. R. *Annu. Rev. Biophys. Biomol. Struct.* **1994**, *23*, 609 (Figure 7).
(30) Rybenkov, V. V.; Cozzarelli, N. R.; Vologodskii, A. V. *Proc. Natl. Acad. Sci. U.S.A.* **1993**, *90*, 5307.
(31) Brian, A. A.; Frisch, H. L.; Lerman, L. S. *Biopolymers* **1981**, *20*, 1305.
(32) Nicolai, T.; Mandel, M. *Macromolecules* **1989**, *22*, 438.
(33) Fixman, M. *J. Chem. Phys.* **1990**, *92*, 6283.
(34) Stigter, D.; Dill, K. A. *J. Phys. Chem.* **1993**, *97*, 12995.
(35) Shaw, S. Y.; Wang, J. C. *Science* **1993**, *260*, 533.
(36) Peitzsch, R. M.; Burt, M. J.; Reed, W. F. *Macromolecules* **1992**, *25*, 806.
(37) Post, C. B. *Biopolymers* **1983**, *22*, 1087.
(38) Manning, G. S. *Biopolymers* **1981**, *20*, 1751.
(39) Carnie, S. L.; Christos, G. A.; Creamer, T. P. *J. Chem. Phys.* **1988**, *89*, 6484.
(40) Christos, G. A.; Carnie, S. L.; Creamer, T. P. *Macromolecules* **1992**, *25*, 1121.
(41) Reed, C. E.; Reed, W. F. *J. Chem. Phys.* **1991**, *94*, 8479.
(42) Krishnaswamy, K.; Fixman, M. *J. Mol. Liq.* **1994**, *61*, 209.
(43) Flory, P. J. *Statistical Mechanics of Chain Molecules*; Interscience: New York, 1969.
(44) Förster, S.; Schmidt, M.; Antonietti, M. *J. Phys. Chem.* **1992**, *96*, 4008.
(45) Hill, T. L. *Statistical Thermodynamics*; Addison-Wesley: Reading, MA, 1960.
(46) Wall, F. T. *J. Chem. Phys.* **1942**, *10*, 132, 485; **1943**, *11*, 527.
(47) Dunn, J. J.; Studier, F. W. *J. Mol. Biol.* **1983**, *166*, 477.
(48) Sobel, E. S.; Harpst, J. A. *Biopolymers* **1991**, *31*, 1559.
(49) Rosenberg, A. H.; Studier, F. W. *Biopolymers* **1969**, *7*, 765.
(50) Borochov, N.; Eisenberg, H.; Kam, Z. *Biopolymers* **1981**, *20*, 231.
(51) Takahashi, A.; Kato, T.; Nagasawa, M. *J. Phys. Chem.* **1967**, *71*, 2001.
(52) Grosberg, A. Yu.; Kuznetsov, D. V. *J. Phys. II Fr.* **1992**, *2*, 1327.
(53) Flory, P. J.; Krigbaum, W. R. *J. Chem. Phys.* **1950**, *18*, 1086.

MA946315E